

Power spectrum of post-inflationary primordial magnetic fields

Héctor J. Hortua*

*Grupo de Gravitación y Cosmología, Observatorio Astronómico Nacional,
Universidad Nacional de Colombia, cra 45 #26-85, Ed. Uriel Gutiérrez, Bogotá D.C, Colombia.
Departamento de Ciencias Básicas, Institución Universitaria Los Libertadores, Cra. 16 # 63A-68, Bogotá, Colombia*

Leonardo Castañeda†

*Grupo de Gravitación y Cosmología, Observatorio Astronómico Nacional,
Universidad Nacional de Colombia, cra 45 #26-85, Ed. Uriel Gutiérrez, Bogotá D.C, Colombia
(Dated: December 6, 2024)*

The origin of large-scale magnetic field is an unsolved problem in modern cosmology. In order to overcome this problem, a possible scenario comes from the idea that these fields emerged from a small primordial field produced in the early universe. This field could lead to the observed large-scales magnetic fields but also, would have left an imprint on the CMB. In this work we summarize some statistical properties of this primordial magnetic fields on the FLRW background Universe. Then, we show the resulting magnetic field power spectrum using the gauge invariant approach in cosmological perturbation theory and we describe some effects of primordial magnetic fields on the CMB anisotropies.

Keywords: Primordial magnetic fields, CMB

arXiv:1405.1786v1 [gr-qc] 8 May 2014

* hjhortuao@unal.edu.co

† lcastanedac@unal.edu.co

I. INTRODUCTION

Magnetic fields have been observed in all scales of the universe, from planets and stars to galaxies and galaxy clusters [1]. However, the origin of such a magnetic field remains as one of the unsolved mysteries in modern cosmology. There is a school of thought which states that magnetic fields we observe today has a primordial origin, indeed, there are some processes in early epoch of the universe that would have created a small magnetic field *a seed* and after a while possibly was amplified by dynamo actions or adiabatic compression during the structure formation era [2]. The origin of this primordial magnetic fields (PMF) can be searched as electroweak and QCD phase transitions, inflation, string theory, among others [10]. Basically we can classify this seed in two groups depending on generation model (Inflation or post-inflation scenarios). If we consider an inflation scenario for example, we can get PMFs on scales larger than the Hubble horizon with a variety of spectral indices (supposing the power spectrum of PMF has the form of a power-law). Whilst post inflationary scenarios, causally PMFs are generated, thus the maximum coherence length for the fields must be no less than Hubble horizon and besides the spectral index is greater than two [11]. If PMFs really were present before to recombination era, these could have some effect on big-bang nucleosynthesis, electroweak baryogenesis process and would leave imprints in the temperature and polarization anisotropies of the cosmic microwave background (CMB) [3]. This effect on CMB has been studied since the early attempts of Zeldovich and nowadays it is a subject of active investigation [4], [5], [6], [7], [9]. In cases where PMF is supposing to be homogeneous, some authors have found these ones can produce effects on acoustic peaks due to fast magnetosonic waves and Alfvén's wave induce correlations in temperature multipole moments [11], [12]. Other alternative is to consider a stochastic PMF with power spectra is assumed to be power law. In this case the Alfvén waves induced by stochastic magnetic field affects the pattern of temperature and B-polarization on CMB [13]. Different works have addressed the study of PMF in scenarios where these are modeled via stochastic fields due to the fact are more realistic and looks like to the ones found in clusters of galaxies [14], [11]. Also, [15] studied the impact of a stochastic PMF on scalar, vector and tensor modes on CMB anisotropies, finding vector modes dominates over the scalar ones at high multipolar numbers and [23], [18] analysed the non-Gaussian signals on CMB generated via stochastic PMFs. In this paper we focus our study in the case of PMF generated in post inflationary stages and their influence in the CMB anisotropies. For this, we calculate the exact scalar, vector and tensor power spectrum for the energy density, Maxwell stress-energy tensor and Lorentz force of a stochastic PMF with a upper cutoff at k_D (which corresponds to the damping scale) and a lower cutoff k_m (which corresponds to the Hubble radius when the field was generated). We also calculate the angular power spectrum of the CMB temperature anisotropy induced by a magnetic perturbation. This paper is organised as follows: Section 2 describes the two-point correlation function for a statistically homogeneous and isotropic magnetic field, Section 3 explains the cutoff in the definitions of the power spectrum, Section 3 presents the integration technique and Section 4 reports numerical solutions of the power spectrum of a PMF. With the exact expression of the power spectrum, the angular power spectrum of the CMB induced by PMFs can be found in Section 5. Finally, a summary of the work and the conclusions are presented in Section 6.

II. MAGNETIC CORRELATION FUNCTIONS

To deal with a PMF, the space-time under study is the fluid permeated by a weak magnetic field, which is a stochastic field and can be treated as a perturbation on a flat-Friedman-Lemaître-Robertson Walker (FLRW) background

$$ds^2 = a^2(\tau) (-d\tau^2 + \delta_{ij} dx^i dx^j), \quad (1)$$

with $a(\tau)$ the scale factor ¹ and where the electromagnetic energy momentum tensor at first order in the perturbation theory is quadratic in the magnetic fields

$$T_{00(B)}(\mathbf{x}, \tau) = \rho_B(\mathbf{x}, \tau) = \frac{1}{8\pi} B^2(\mathbf{x}, \tau), \quad (2)$$

$$T_{ij(B)}(\mathbf{x}, \tau) = \frac{1}{4\pi} \left[B_i(\mathbf{x}, \tau) B_j(\mathbf{x}, \tau) - \frac{1}{3} \delta_{ij} B^2(\mathbf{x}, \tau) \right], \quad (3)$$

also, the anisotropic trace-free part of the stress-energy tensor (spatial part of energy momentum tensor) of the magnetic field takes the form

$$\Pi_{ij}(\mathbf{x}, \tau) = T_{ij(B)}(\mathbf{x}, \tau) + \frac{1}{3} \delta_{ij} \rho_B(\mathbf{x}, \tau). \quad (4)$$

¹ Hereafter the Greek indices run from 0 to 3, and the Latin ones run from 1 to 3, we will work with conformal time τ , τ_0 is the current value of conformal time.

The PMF amplitud scales as $B^2(\mathbf{x}, t) = \frac{B(\mathbf{x})}{a^4(\tau)}$ at larges scales within the infinite conductivity limit which is a good approximation before the decoupling epoch.

A. The statistics for a stochastic PMF

Now, the PMF power spectrum which is defined as the Fourier Transform of the two points correlation can be written as

$$\langle B_i^*(\mathbf{k})B_j(\mathbf{k}') \rangle = (2\pi)^3 \delta^3(\mathbf{k} - \mathbf{k}') P_{ij} P_B(\mathbf{k}), \quad (5)$$

where P_{ij} is a projector onto the transverse plane², $P_B(\mathbf{k})$ is the PMF power spectrum and where we use the Fourier transform conventions

$$B_j(\mathbf{x}) = \int \frac{d^3x}{(2\pi)^3} \exp(-i\mathbf{k} \cdot \mathbf{x}) B_j(\mathbf{k}) \quad \text{and} \quad \delta(\mathbf{k}) = \int \frac{d^3x}{(2\pi)^3} \exp(i\mathbf{k} \cdot \mathbf{x}). \quad (6)$$

Since B is statistically homogeneous and isotropic, the correlation depends only on the distance $|\mathbf{x} - \mathbf{y}|$. We restrict our attention to the evolution of a causally-generated PMF parametrized by the power law with index $n \geq 2$, with an ultraviolet cutoff k_D and the dependence of an infrared cutoff, k_m , thus, we consider for $k_m \leq k \leq k_D$, the power spectrum can be defined as

$$P_B(k) = Ak^n, \quad (7)$$

with A , being the normalization constant which is found by [11] to be

$$A = \frac{B_\lambda^2 2\pi^2 \lambda^{n+3}}{\Gamma(\frac{n+3}{2})}, \quad (8)$$

where B_λ is the comoving PMF strength smoothing over a Gaussian sphere of comoving radius λ . The equations, for energy density of magnetic field and anisotropic trace-free part respectively written in Fourier space are

$$\rho_B(k, \tau) = \frac{1}{8\pi} \int \frac{d^3k'}{(2\pi)^3} B_l(k) B^l(k - k'), \quad (9)$$

$$\Pi_{ij}(k, \tau) = \frac{1}{4\pi} \int \frac{d^3k'}{(2\pi)^3} \left[B_i(k') B_j(k - k') - \frac{1}{3} \delta_{ij} B_l(k') B^l(k - k') \right]. \quad (10)$$

Following [20], the anisotropic trace-free part can be splitted in a scalar, vector and tensor part

$$\Pi^{(S)}(k, \tau) = \frac{3}{2} \left(\frac{\mathbf{k}_i \mathbf{k}_j}{k^2} - \frac{1}{3} \delta_{ij} \right) \Pi^{ij}(k, \tau), \quad (11)$$

$$\Pi_i^{(V)}(k, \tau) = P_{ij} \frac{\mathbf{k}_l}{k} \Pi^{lj}(k, \tau), \quad (12)$$

$$\Pi_{ij}^{(T)}(k, \tau) = \left(P_{il} P_{jm} - \frac{1}{2} P_{ij} P_{lm} \right) P^{mn} P^{ls} \Pi_{ns}(k, \tau), \quad (13)$$

where they scale in the same way that energy density of PMF like $\Pi_{ij}(k, \tau) = \frac{\Pi_{ij}(k, \tau_0)}{a^4(\tau)}$. Furthermore, PMFs affect motions of ionized baryons by the Lorentz force which is read as

$$\mathbf{L}(k, \tau_0) = \frac{1}{4\pi} ((\nabla \times \mathbf{B}(\mathbf{x})) \times \mathbf{B}(\mathbf{x})), \quad (14)$$

which appears in the Navier-stokes equation at first order when PMF is considered [21]. Using the free divergence of magnetic field property and the decomposition the Lorentz force into a scalar and vector part, the relation between the anisotropic stress-energy tensor and Lorentz force is given by

$$\Pi^{(S)}(\mathbf{x}, \tau_0) = L^{(S)}(\mathbf{x}, \tau_0) + \frac{1}{3} \rho_B(\mathbf{x}, \tau_0). \quad (15)$$

² Being $P_{ij} = \delta_{ij} - \frac{\mathbf{k}_i \mathbf{k}_j}{k^2}$, where $P_{ij} P_{jk} = P_{ik}$ and $P_{ij} \mathbf{k}_j = 0$.

Now, we use the two point correlation function for $\rho_B(k, \tau)$, $\Pi(k, \tau)$, $L_B(k, \tau)$ and the cross correlation between them

$$\langle \rho_B(k, \tau) \rho_B^*(k', \tau) \rangle = (2\pi)^3 |\rho_B(k, \tau)|^2 \delta^3(k - k'), \quad (16)$$

$$\langle \Pi^{(S)}(k, \tau) \Pi^{(S)*}(k', \tau) \rangle = (2\pi)^3 \left| \Pi^{(S)}(k, \tau) \right|^2 \delta^3(k - k'), \quad (17)$$

$$\langle L^{(S)}(k, \tau) L^{(S)*}(k', \tau) \rangle = (2\pi)^3 \left| L^{(S)}(k, \tau) \right|^2 \delta^3(k - k'), \quad (18)$$

$$\langle \rho_B(k, \tau) L^{(S)*}(k', \tau) \rangle = (2\pi)^3 \left| \rho_B(k, \tau) L^{(S)}(k, \tau) \right| \delta^3(k - k'), \quad (19)$$

$$\langle \rho_B(k, \tau) \Pi^{(S)}(k', \tau) \rangle = (2\pi)^3 \left| \rho_B(k, \tau) \Pi^{(S)}(k, \tau) \right| \delta^3(k - k'), \quad (20)$$

for the scalar part. For the vector and tensor part we have

$$\langle \Pi_i^{(V)}(k, \tau) \Pi_j^{(V)*}(k', \tau) \rangle = (2\pi)^3 P_{ij} \left| \Pi^{(V)}(k, \tau) \right|^2 \delta^3(k - k'), \quad (21)$$

$$\langle \Pi_{ij}^{(T)}(k, \tau) \Pi_{ij}^{(T)*}(k', \tau) \rangle = 4(2\pi)^3 \left| \Pi^{(T)}(k, \tau) \right|^2 \delta^3(k - k'), \quad (22)$$

respectively, here the power spectrum depend only on $k = |\mathbf{k}|$. Now, to calculate the power spectrum, we substitute the equations (9) and (10) in the above expressions, then we use the Wick's theorem to evaluate the 4-point correlator of the PMF and finally the equation (5) is used. After a straightforward but somewhat lengthy calculation one obtains the power spectrum for $\rho_B(k, \tau)$, $\Pi(k, \tau)$, $L_B(k, \tau)$ given by

$$|\rho_B(k, \tau)|^2 = \frac{1}{256\pi^5} \int d^3k' (1 + \mu^2) P_B(k') P_B(|\mathbf{k} - \mathbf{k}'|), \quad (23)$$

$$\left| L^{(S)}(k, \tau) \right|^2 = \frac{1}{256\pi^5} \int d^3k' [4(\gamma^2 \beta^2 - \gamma \mu \beta) + 1 + \mu^2] P_B(k') P_B(|\mathbf{k} - \mathbf{k}'|), \quad (24)$$

$$\left| \Pi^{(s)}(k, \tau) \right|^2 = \frac{1}{576\pi^5} \int d^3k' [4 - 3(\beta^2 + \gamma^2) + \mu^2 + 9\gamma^2 \beta^2 - 6\mu \beta \gamma] P_B(k') P_B(|\mathbf{k} - \mathbf{k}'|), \quad (25)$$

for scalar modes

$$\left| \rho_B(k, \tau) L^{(S)}(k, \tau) \right| = \frac{1}{256\pi^5} \int d^3k' [1 - 2(\gamma^2 + \beta^2) + 2\gamma \mu \beta - \mu^2] P_B(k') P_B(|\mathbf{k} - \mathbf{k}'|), \quad (26)$$

$$\left| \rho_B(k, \tau) \Pi^{(S)}(k, \tau) \right| = \frac{1}{128\pi^5} \int d^3k' \left[\frac{2}{3} - (\gamma^2 + \beta^2) + \mu \gamma \beta - \frac{1}{3} \mu^2 \right] P_B(k') P_B(|\mathbf{k} - \mathbf{k}'|), \quad (27)$$

for the scalar cross correlation and

$$\left| \Pi^{(V)}(k, \tau) \right|^2 = \frac{1}{128\pi^5} \int d^3k' [(1 + \beta^2)(1 - \gamma^2) + \mu \gamma \beta - \gamma^2 \beta^2] P_B(k') P_B(|\mathbf{k} - \mathbf{k}'|), \quad (28)$$

$$\left| \Pi^{(T)}(k, \tau) \right|^2 = \frac{1}{512\pi^5} \int d^3k' [1 + 2\gamma^2 + \gamma^2 \beta^2] P_B(k') P_B(|\mathbf{k} - \mathbf{k}'|), \quad (29)$$

for the vector and tensor part. The angular functions are defined as

$$\beta = \frac{\mathbf{k} \cdot (\mathbf{k} - \mathbf{k}')}{k |\mathbf{k} - \mathbf{k}'|}, \quad \mu = \frac{\mathbf{k}' \cdot (\mathbf{k} - \mathbf{k}')}{k' |\mathbf{k} - \mathbf{k}'|}, \quad \gamma = \frac{\mathbf{k} \cdot \mathbf{k}'}{kk'}. \quad (30)$$

Our results are in agreement with those found by [20], [16], [5].

III. THE CUTOFF DEPENDENCE WITH THE SCALE

In this part we solve the last expressions for getting the power spectrum of a causal PMF generated before recombination epoch. In the cosmological scenario, in considering a stochastic PMF a upper cutoff k_D corresponds to the damping scale should be taking in account, in sense that magnetic field energy is dissipated into heat through the damping of magnetohydrodynamics waves. The damping occurs due to the diffusion of neutrinos prior to neutrino decoupling ($T \sim 1\text{MeV}$) and the photons before recombination ($T \sim 0.25\text{ eV}$). Particularly, we try with three types of propagating MHD modes, the fast and slow magnetosonic waves and the Alfvén waves [11], [17]. However, we concentrate in the latter because these ones are the most effective in damping when radiation is free-streaming (recombination), that is, when $k \leq V_A L_{Silk}$, where V_A is the Alfvén speed and L_{Silk} , the Silk damping scale at recombination, [22], [23]. The upper cutoff of PMF was found by [22], [11] which is dependent of strength of magnetic energy and the spectral index as follows

$$k_D \approx (1.7 \times 10^2)^{\frac{2}{n+5}} \left(\frac{B_\lambda}{10^{-9}nG} \right)^{\frac{-2}{n+5}} \left(\frac{k_\lambda}{1Mpc^{-1}} \right)^{\frac{n+3}{n+5}} h^{\frac{1}{n+5}} Mpc^{-1}, \quad (31)$$

where $h = 0.679 \pm 0.100$. On the other hand, tensor modes suffer more damping at equality epoch ($T \sim 3\text{eV}$) and the cutoff takes the following form

$$k_D \approx (8.3 \times 10^3)^{\frac{2}{n+5}} \left(\frac{B_\lambda}{10^{-9}nG} \right)^{\frac{-2}{n+5}} \left(\frac{k_\lambda}{1Mpc^{-1}} \right)^{\frac{n+3}{n+5}} h^{\frac{6}{n+5}} Mpc^{-1}, \quad (32)$$

Therefore, the damping scale changes with time and the power spectrum for a PMF must have a time dependence due to the cosmic epoch where it is present besides the decay by the expansion of the universe. With the latter equations, we can expect a high contribution of tensor modes on CMB for large scales respect to the vector ones. Now, the power law spectrum of magnetic field more general we want to study takes account a infrared cutoff k_m for low values of k and which depend on the generation model of PMF. This minimal scale has been studied by [7], [8], [19] for showing the effects of PMF on abundances of primordial light elements using Big bang nucleosynthesis (BBN), the distortions on CMB due to a background PMF and the relevance of PMF in formation of structure in the universe respectively. Therefore, our interesting scale k moves from k_m to k_D and we approximate this infrared cut off as $k_m = \alpha k_D$ where $0 < \alpha < 1$. For the calculation, in the magnetic energy density the field varies from $1nG$ to $10nG$, $\alpha = 0.001$ and the physically interesting region of spectra is realized when $n \geq 2$ (blue spectral).

A. Integration method

We choose our coordinate system in such a way that \mathbf{k} is along the \mathbf{z} axis, thus γ is the cosine of angle between \mathbf{k}' and the \mathbf{z} axis ($\gamma = \cos\theta$). The integration measure can be written, in spherical coordinates as $d^3k' = k'^2 dk' d\gamma d\phi$. The angular part related with ϕ is just equal to 2π . But, there is a constraint on the angle to be integrated over γ , depending on the magnitude of \mathbf{k}' . For making the integration two conditions need to be taken into account

$$k_m < |\mathbf{k} - \mathbf{k}'| < k_D, \quad k_m < |\mathbf{k}'| < k_D. \quad (33)$$

Under these conditions, the power spectra to be non zero only for $0 < k < 2k_D$. The integration domain for calculating the power spectrum is found in appendix A.

IV. PMF POWER SPECTRA

In figure 1 we show the magnetic energy density convolution and its dependence with the spectral index and the amplitude of PMF at a scale of $\lambda = 1\text{Mpc}$ (we plot the power spectra times k^3 for comparing with [16]). We note that the amplitude of the spectra is proportional not only with the strength of PMF as well to spectral index. The effect of the smoothing scale over power spectrum is shown in figure 2, where we fix the strength of the field at $1nG$. In the figure 3 the Lorentz force spectra is shown with varying n keeping an amplitude of $B_\lambda^2 = 1nG$ at a scale of $\lambda = 1\text{Mpc}$. The scalar, vector and tensor anisotropic modes are shown in figure 4. In this plot we can see that largest contribution comes from tensor modes followed by scalar modes over the vector ones. Also we can check the dependence with the spectral index for an amplitude of $B_\lambda = 1nG$ and $\lambda = 1\text{Mpc}$. In figure 5 we show the cross correlation between the energy density with Lorentz force and anisotropic trace-free part, we note that the cross correlation is negative in all

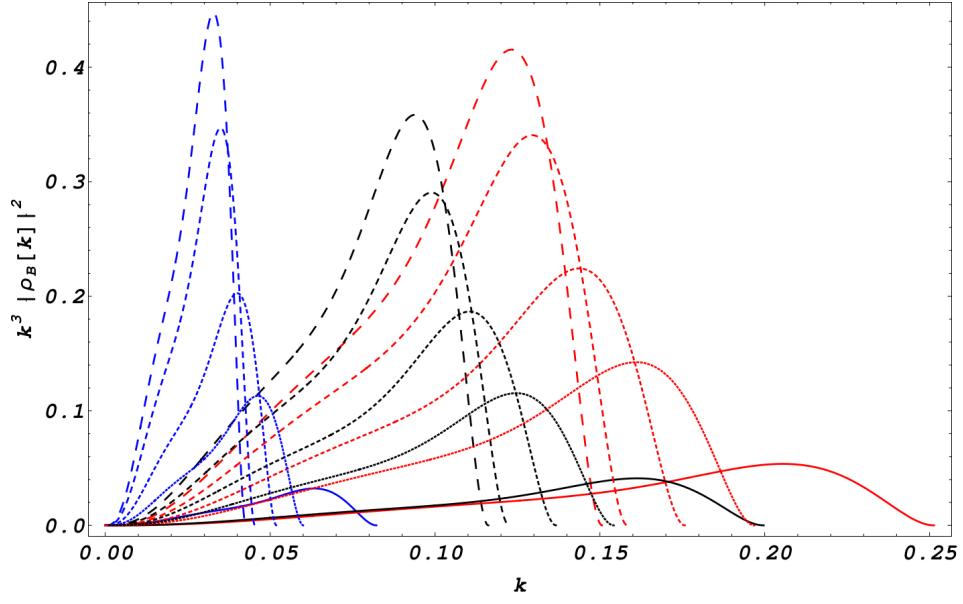


FIG. 1. Plot of magnetic energy density of PMF power spectrum $k^3 |\rho_B(k, \tau)|^2$ versus k for different values of amplitude of PMF, B_λ^2 (thick for $B = 1nG$, large dashed for $10nG$, tiny dashed for $3nG$, small dashed for $5nG$ and medium dashed for $8nG$) and different spectral index ($n = 2$ for blue, $n = 7/2$ for black and $n = 4$ for red).

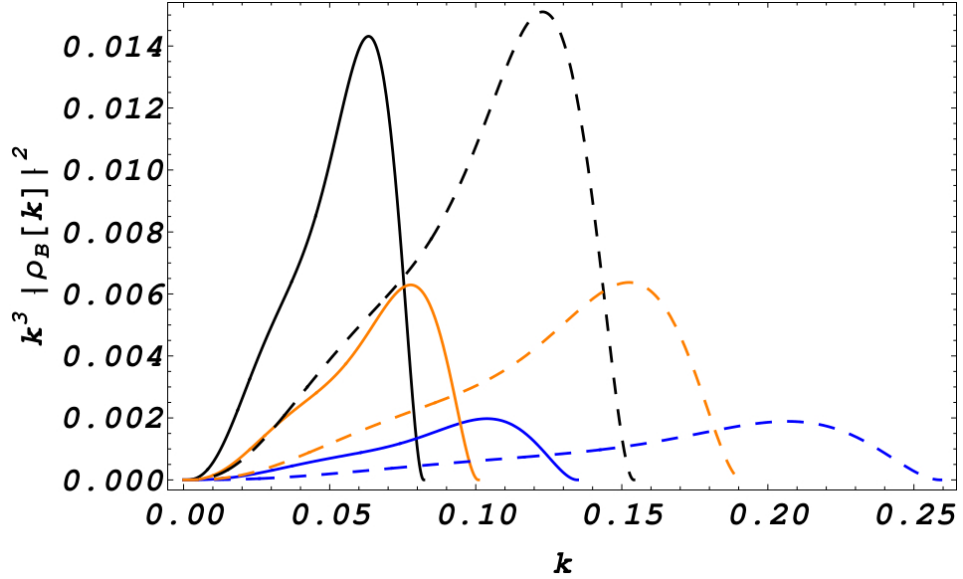


FIG. 2. Plot of magnetic energy density of PMF power spectrum $k^3 |\rho_B(k, \tau)|^2$ versus k for different values of smoothing scale (black for $\lambda = 1\text{Mpc}$, orange for $\lambda = 0.75\text{Mpc}$ and blue for $\lambda = 0.5\text{Mpc}$) and for different spectral index ($n = 2$ for thick lines and $n = 3$ for dashing large lines).

range of scales for the first case whilst the second case the it starts to be negative for values of $k \geq 0.05$ (with $n = 3$) and $k \geq 0.03$ (with $n = 2$). The figure 6 shows a comparison of our results of vector and tensor anisotropic trace-free parts with the found by [15] (see figure 1 and equation (A2) in this paper) and [11] (see equations (2.18), (2.22) in this paper) where for the values $B_\lambda = 1nG$, $n = 2$ and $\lambda = 1\text{Mpc}$. We can observe our results are in agreement with first authors and are in concordance with the second ones just for $k \leq 0.015$ for vector modes and $k \leq 0.005$ for tensor modes. The scale k for this plot runs from 0 to $k_D \sim 0.04$ in sense that result found by [11] is valid for this range. Finally, since the cut off are dependent from the generation of the PMF, it is important to study how affects the lower cut-off k_m to power spectrum. For this, we plot in figure 7 the power spectrum for different values of k_m . Here we can see the strong dependence of the power spectrum with this scale, basically the power spectrum does not change

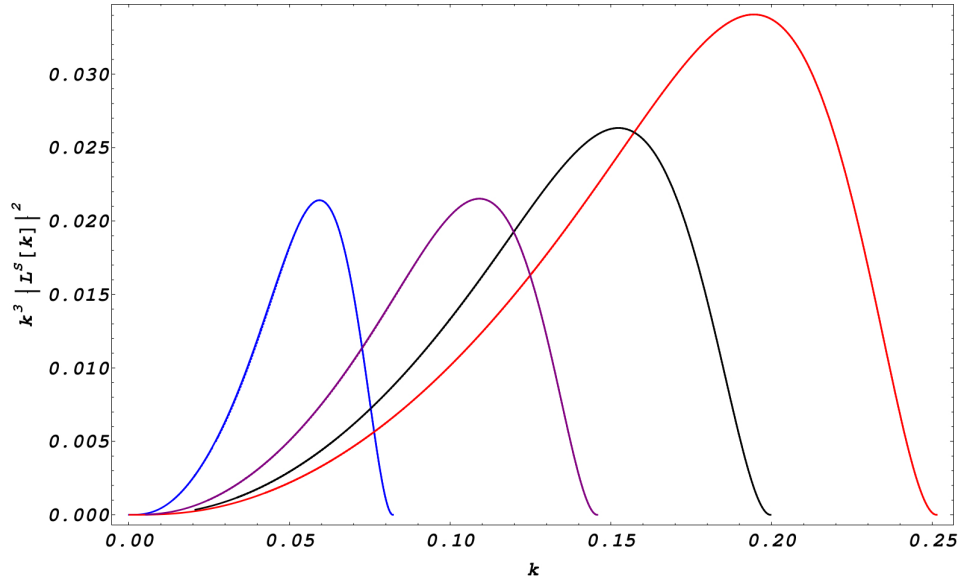


FIG. 3. Plot of Lorentz force spectra $k^3 |L^{(S)}(k, \tau)|^2$ versus k for different spectral index ($n = 2$ for blue, $n = 3$ for purple, $n = 7/2$ for black and $n = 4$ for red).

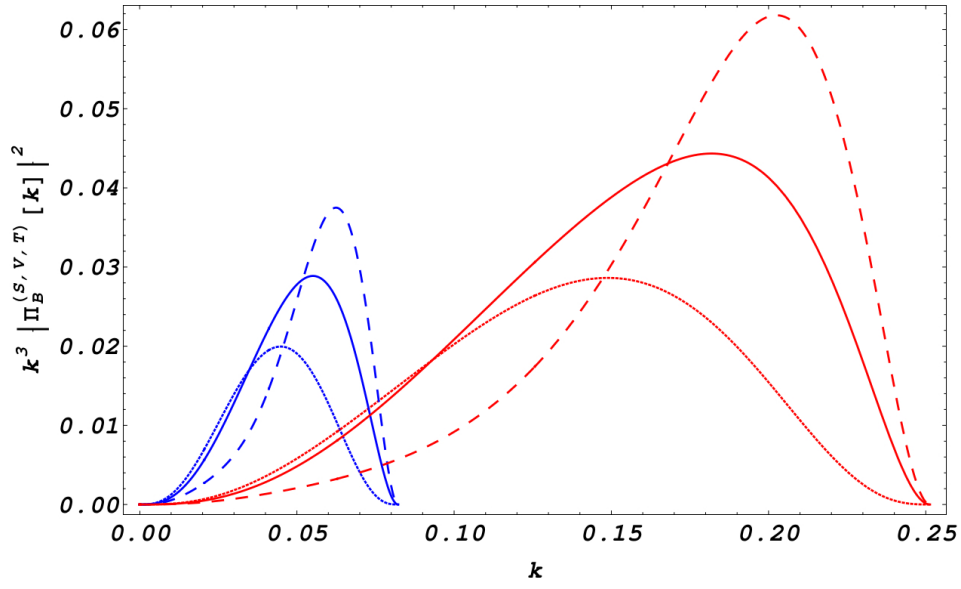


FIG. 4. Plot of scalar (thick), vector (short dashed) and tensor (large dashed) parts of the anisotropic trace-free part power spectrum $k^3 |\Pi(k, \tau)|^2$ versus k for different spectral index ($n = 2$ for blue and $n = 4$ for red).

when $0.2k_D > k_m > 0$ with respect to the results of $k_m = 0$, but in the cases where $k_m > 0.2k_D$ there is a significant variation with a zero lower cutoff.

V. CMB POWER SPECTRA

Using the total angular momentum formalism introduced by [24], the angular power spectrum of the CMB temperature anisotropy is given as

$$(2l+1)^2 C_l^{\Theta\Theta} = \frac{2}{\pi} \int \frac{dk}{k} \sum_{m=-2}^2 k^3 \Theta_l^{(m)*}(\tau_0, k) \Theta_l^{(m)}(\tau_0, k), \quad (34)$$

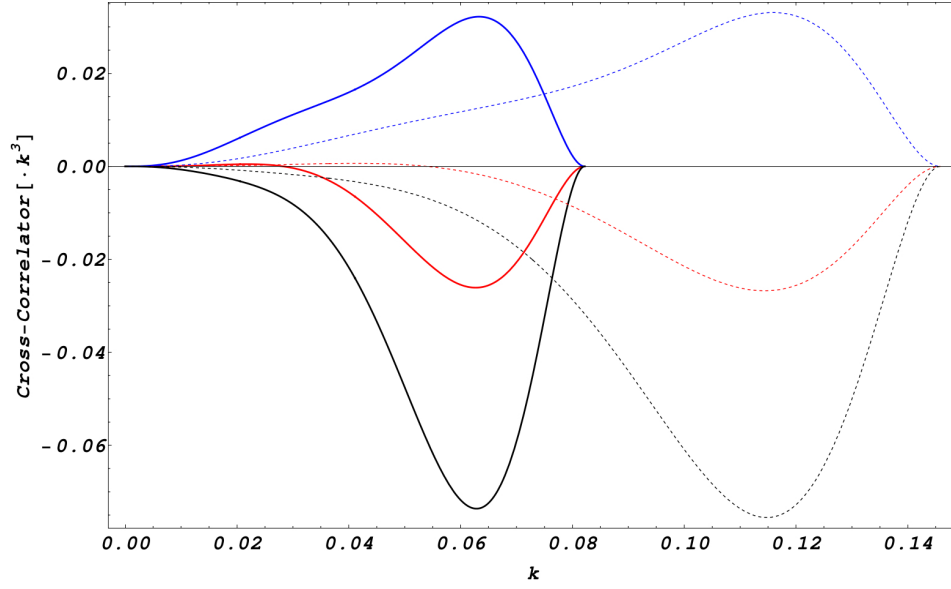


FIG. 5. Plot of correlation of $k^3 |\rho_B(k, \tau) \Pi^{(S)}(k, \tau)|$ in red, $k^3 |\rho_B(k, \tau) L^{(S)}(k, \tau)|$ in black and $k^3 |\rho_B(k, \tau)|^2$ in blue, for different spectral index ($n = 2$ for thick line and $n = 3$ for short dashed).

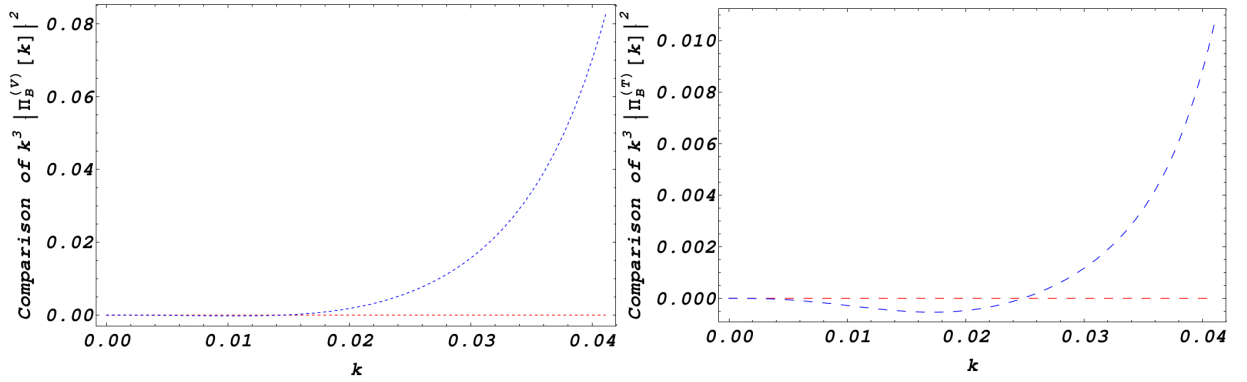


FIG. 6. Plot of comparison between our results of the anisotropic trace-free part power spectrum $k^3 |\Pi^{(S,V)}(k, \tau)|^2$ versus [15] (red) and [11] (blue) for values of $n = 2$, $B = 1nG$ and $\lambda = 1Mpc$.

where $m = 0, \pm 1, \pm 2$ are the scalar, vector and tensor perturbations modes and $\Theta_l^{(m)}(\tau_0, k)$ are the temperature fluctuation $\frac{\delta T}{T}$ multipolar moments. In large scales, one can neglected the contribution on CMB temperature anisotropies by ISW effect in presence of a PMF. Therefore, considering just the fluctuation via PMF perturbation, [11] found that temperature anisotropy multipole moment for $m = 0$ becomes

$$\frac{\Theta_l^{(S)}(\tau_0, k)}{2l+1} \approx \frac{-8\pi G}{3k^2 a_{dec}^2} \rho_B(\tau_0, k) j_l(k\tau_0), \quad (35)$$

where a_{dec} is the value of scalar factor at decoupling, G is the Gravitational constant and j_l is the spherical Bessel function. Substituting the last expression in equation (34), the CMB temperature anisotropy angular power spectrum is given by

$$l^2 C_l^{\Theta\Theta(S)} = \frac{2}{\pi} \left(\frac{8\pi G}{3a_{dec}^2} \right)^2 \int_0^\infty \frac{|\rho_B(\tau_0, k)|^2}{k^2} j_l^2(k\tau_0) l^2 dk, \quad (36)$$

where for our case, we should integrate only up to $2k_D$ since it is the range where energy density power spectrum is not zero. The result of the angular power spectrum induced by scalar magnetic perturbations given by equation (36)

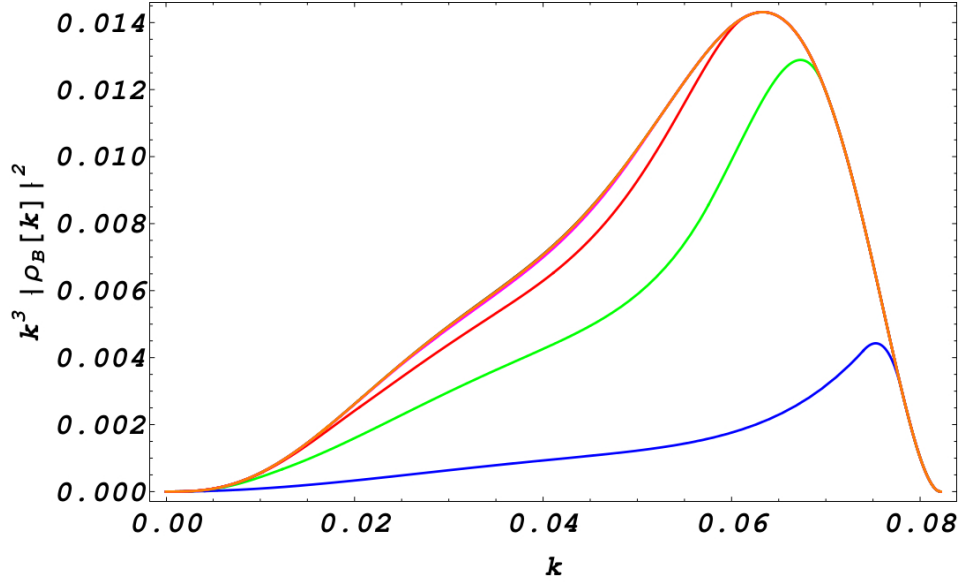


FIG. 7. Plot of magnetic energy density of PMF power spectrum $k^3 |\rho_B(k, \tau)|^2$ versus k for different values of cutoff (blue for $k_m = 0.9k_D$, green for $k_m = 0.7k_D$, red for $k_m = 0.5k_D$, magenta for $k_m = 0.3k_D$, orange for $k_m = 0.2k_D$, brown for $k_m = 0.1k_D$ and black for $k_m = 0.01k_D$).

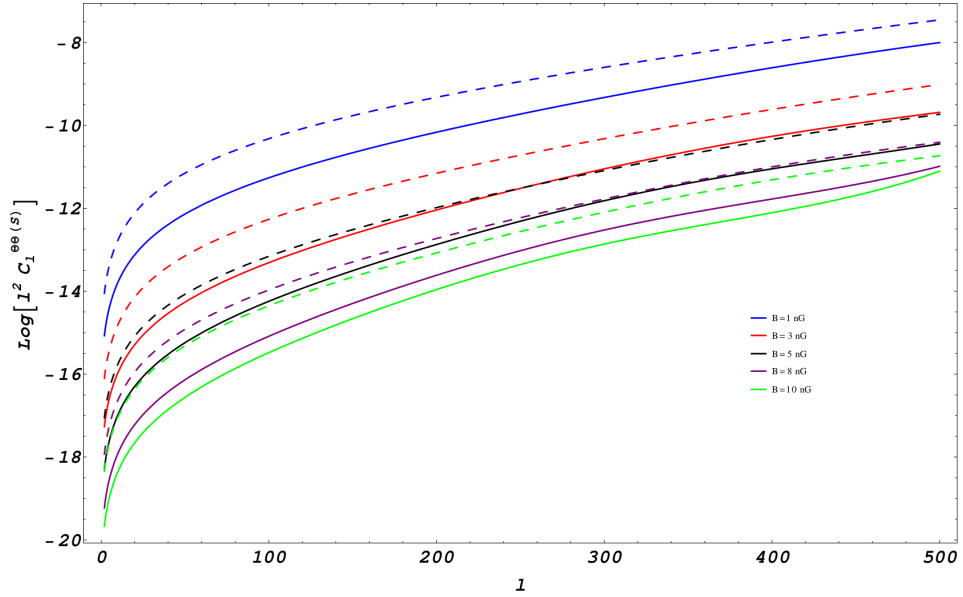


FIG. 8. Plot of the CMB temperature anisotropy angular power spectrum induced by scalar magnetic perturbations, where the thick lines is for $n = 2$ and the large dashed for $n = 5/2$.

is shown in the figure 8. Here, the color labeled in the graphic denote the strength of PMF and the thick lines show the power spectrum for $n = 2$ and the dashes lines for $n = 5/2$, we plot the $\log l^2 C_l^{\Theta\Theta}$ in order to compare with other results.

In the case where $m \pm 2$ (tesor modes), the temperature anisotropy multipole moment is given by Eq. (5.22) of [11]

$$\frac{\theta_l^{(T)}}{2l+1} \simeq -2\pi \sqrt{\frac{8(l+2)!}{3(l-2)!}} \left(G\tau_0^2 z_{eq} \ln \left(\frac{z_{in}}{z_{eq}} \right) \right) \Pi^{(T)}(k, \tau_0) \int_0^{x_0} \frac{j_2(x)}{x} \frac{j_l(x_0 - x)}{(x_0 - x)^2} dx, \quad (37)$$

where z_{in} and z_{eq} are the redshift when PMF was created (during the radiation dominated era) and equal matter and radiation era respectively (it's assumed that $\frac{z_{in}}{z_{eq}} \sim 10^9$) and $x_0 = k\tau_0$. For the integral found in the last expression,

we use the approximation made by [12]

$$\int_0^{x_0} \frac{j_2(x)}{x} \frac{j_l(x_0 - x)}{(x_0 - x)^2} dx \simeq \frac{7\pi}{25} \frac{\sqrt{l}}{x_0^3} J_{l+3}(x_0), \quad (38)$$

where $j_l(z) = \sqrt{\frac{\pi}{2z}} J_{l+\frac{1}{2}}(z)$. With this approximation the tensor CMB temperature anisotropy angular power spectrum induced by a PMF is given by

$$l^2 C_l^{\Theta\Theta(T)} = 1.25\pi^3 \left(G z_{eq} \ln \left(\frac{z_{in}}{z_{eq}} \right) \right)^2 \frac{l^4(l-1)(l+1)(l+2)}{(2l+1)^2 \tau_0^2} \int \frac{dk}{k^4} J_{l+3}^2(k\tau_0) \left| \Pi^{(T)}(k, \tau_0) \right|^2. \quad (39)$$

The plot of CMB power spectra for tensor perturbations from a power-law stochastic PMF with spectral index $n = 2$ (thick lines) and $n = 4$ (dashed lines) for different amplitudes of magnetic field is shown in figure 9.

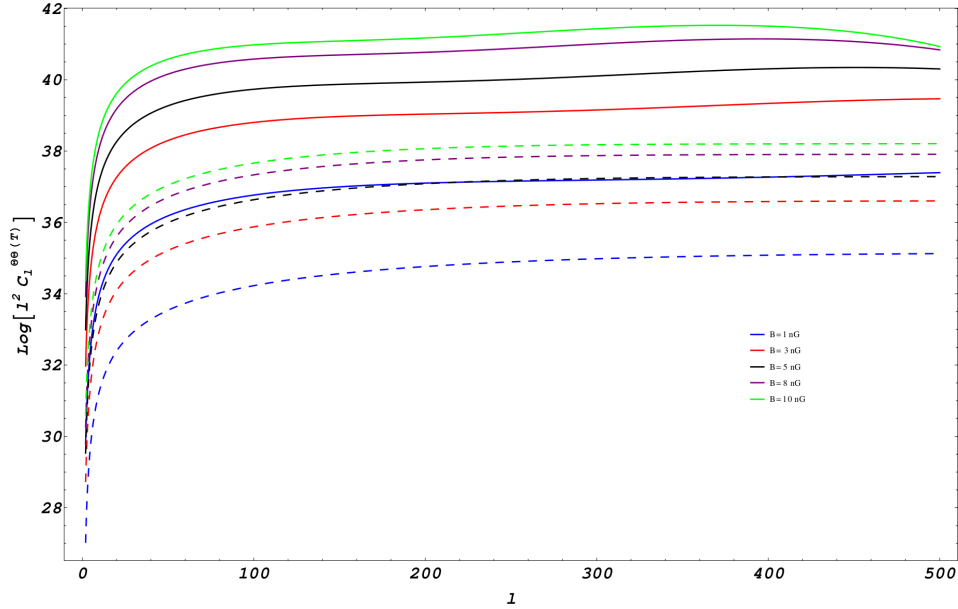


FIG. 9. Plot of the CMB temperature anisotropy angular power spectrum induced by tensor magnetic perturbations, where the thick lines is for $n = 2$ and the large dashed for $n = 4$.

VI. DISCUSSION

PMFs induce scalar, vector and tensor fluctuations on CMB temperature anisotropies. In this paper we show how PMFs could leave imprint on CMB, for this first of all we calculate the exact estimate of the convolution of the Fourier spectra for scalar, vector and tensor modes which was also solved by [16] and [11]. This PMF can be characterized via amplitude of the field and the spectral index in according to the generation model, supposing a power law scaling. Here we show the power spectra in cases where PMF has been created in the causal horizon, therefore we study the effect created by causal PMF with the property $n \geq 2$, and where amplitude is determined by an upper cutoff (due to damped on small scales by radiation viscosity) and a lower cut off determined by the causal horizon size.

Appendix A: Integration domain

The conditions over k equation (33), introduce a dependence on the angular integration domain and the two allow the energy power spectrum to be non zero only for $0 < k < 2k_D$. The conditions split the double integral in the following form, for $0.2k_D > k_m > 0$ we have

$$2k_m > k > 0$$

$$\int_{k_m}^{k+k_m} d^3k' \int_{-1}^{\frac{k^2+k'^2-k_m^2}{2kk'}} d\gamma + \int_{k_m+k}^{k_D-k} d^3k' \int_{-1}^1 d\gamma + \int_{k_D-k}^{k_D} d^3k' \int_{\frac{k^2+k'^2-k_D^2}{2kk'}}^1 d\gamma \quad (\text{A1})$$

$$\frac{k_D - k_m}{2} > k > 2k_m$$

$$\begin{aligned} & \int_{k_m}^{k-k_m} d^3k' \int_{-1}^1 d\gamma + \int_{k_m+k}^{k_D-k} d^3k' \int_{-1}^1 d\gamma \\ & + \int_{k-k_m}^{k+k_m} d^3k' \int_{-1}^{\frac{k^2+k'^2-k_m^2}{2kk'}} d\gamma + \int_{k_D-k}^{k_D} d^3k' \int_{\frac{k^2+k'^2-k_D^2}{2kk'}}^1 d\gamma \end{aligned} \quad (\text{A2})$$

$$\frac{k_D + k_m}{2} > k > \frac{k_D - k_m}{2}$$

$$\begin{aligned} & \int_{k_m}^{k-k_m} d^3k' \int_{-1}^1 d\gamma + \int_{k-k_m}^{k_D-k} d^3k' \int_{-1}^{\frac{k^2+k'^2-k_m^2}{2kk'}} d\gamma \\ & + \int_{k_D-k}^{k+k_m} d^3k' \int_{\frac{k^2+k'^2-k_D^2}{2kk'}}^{\frac{k^2+k'^2-k_m^2}{2kk'}} d\gamma + \int_{k_m+k}^{k_D} d^3k' \int_{\frac{k^2+k'^2-k_D^2}{2kk'}}^1 d\gamma \end{aligned} \quad (\text{A3})$$

$$k_D - k_m > k > \frac{k_D + k_m}{2}$$

$$\begin{aligned} & \int_{k_m}^{k_D-k} d^3k' \int_{-1}^1 d\gamma + \int_{k_D-k}^{k-k_m} d^3k' \int_{\frac{k^2+k'^2-k_D^2}{2kk'}}^1 d\gamma \\ & + \int_{k-k_m}^{k+k_m} d^3k' \int_{\frac{k^2+k'^2-k_D^2}{2kk'}}^{\frac{k^2+k'^2-k_m^2}{2kk'}} d\gamma + \int_{k_m+k}^{k_D} d^3k' \int_{\frac{k^2+k'^2-k_D^2}{2kk'}}^1 d\gamma \end{aligned} \quad (\text{A4})$$

$$k_D + k_m > k > k_D - k_m$$

$$\int_{k_m}^{k-k_m} d^3k' \int_{\frac{k^2+k'^2-k_D^2}{2kk'}}^1 d\gamma + \int_{k-k_m}^{k_D} d^3k' \int_{\frac{k^2+k'^2-k_D^2}{2kk'}}^{\frac{k^2+k'^2-k_m^2}{2kk'}} d\gamma \quad (\text{A5})$$

$$2k_D > k > k_D + k_m$$

$$\int_{k-k_D}^{k_D} d^3k' \int_{\frac{k^2+k'^2-k_D^2}{2kk'}}^1 d\gamma. \quad (\text{A6})$$

For the case where $k_D > k_m > 0.2$, we have

$$\frac{k_D - k_m}{2} > k > 0$$

$$\int_{k_m}^{k+k_m} d^3k' \int_{-1}^{\frac{k^2+k'^2-k_m^2}{2kk'}} d\gamma + \int_{k_m+k}^{k_D-k} d^3k' \int_{-1}^1 d\gamma + \int_{k_D-k}^{k_D} d^3k' \int_{\frac{k^2+k'^2-k_D^2}{2kk'}}^1 d\gamma \quad (\text{A7})$$

$$k_D - k_m > k > \frac{k_D - k_m}{2}$$

$$\int_{k_m}^{k-k_m} d^3 k' \int_{-1}^{\frac{k^2+k'^2-k_m^2}{2kk'}} d\gamma + \int_{k_D-k}^{k_m+k} d^3 k' \int_{\frac{k^2+k'^2-k_D^2}{2kk'}}^{\frac{k^2+k'^2-k_m^2}{2kk'}} d\gamma + \int_{k+k_m}^{k_D} d^3 k' \int_{\frac{k^2+k'^2-k_D^2}{2kk'}}^1 d\gamma \quad (\text{A8})$$

$$2k_m > k > k_D - k_m$$

$$\int_{k_m}^{k_D} d^3 k' \int_{\frac{k^2+k'^2-k_D^2}{2kk'}}^{\frac{k^2+k'^2-k_m^2}{2kk'}} d\gamma \quad (\text{A9})$$

$$k_m + k_D > k > 2k_m$$

$$\int_{k-k_m}^{k_D} d^3 k' \int_{\frac{k^2+k'^2-k_D^2}{2kk'}}^{\frac{k^2+k'^2-k_m^2}{2kk'}} d\gamma + \int_{k_m}^{k-k_m} d^3 k' \int_{\frac{k^2+k'^2-k_D^2}{2kk'}}^1 d\gamma \quad (\text{A10})$$

$$2k_D > k > k_m + k_D$$

$$\int_{k-k_D}^{k_D} d^3 k' \int_{\frac{k^2+k'^2-k_D^2}{2kk'}}^1 d\gamma. \quad (\text{A11})$$

In the case where $k_m = 0$, the integration domain leads to

$$k_D > k > 0$$

$$\int_0^{k_D-k} d^3 k' \int_{-1}^1 d\gamma + \int_{k_D-k}^{k_D} d^3 k' \int_{\frac{k^2+k'^2-k_D^2}{2kk'}}^1 d\gamma \quad (\text{A12})$$

$$2k_D > k > k_D$$

$$\int_{k-k_D}^{k_D} d^3 k' \int_{\frac{k^2+k'^2-k_D^2}{2kk'}}^1 d\gamma, \quad (\text{A13})$$

which is in agreement with [16].

-
- [1] Lawrence M. W. 2002, *Rev.Mod.Phys*, 74, 775
 - [2] Kandus A., Kunze K.E. & Tsagas C. G. 2012, *Phys.Rept.*, 505, 1
 - [3] Grasso D. & Rubinstein H. R. 2001, *Phys.Rept.*, 348, 163
 - [4] Giovannini M. 2004, *Phys. Rev. D.*, 70, 123507
 - [5] Shaw J. R. & Lewis A. 2010, *Phys. Rev. D.*, 81, 043517
 - [6] Kunze K. E. 2011, *Phys. Rev. D.*, 83, 023006
 - [7] Yamazaki D. G., Ichiki K., Kajino T. & Mathews G. J. 2008, *Phys. Rev. D.*, 77, 043005

- [8] Yamazaki D. G. 2014, *Phys. Rev. D.*, 89, 083528
- [9] Durrer R. 2007, *New.Astron.Rev.*, 51, 275
- [10] Giovannini M. 2006, *Lect. NotesPhys.*, 737, 863
- [11] Mack A., Kahniashvili T. & Kosowsky A. 2002, *Phys. Rev. D.*, 65, 123004
- [12] Durrer R., Kahniashvili T. & Yates A. 1998, *Phys. Rev. D.*, 58, 123004
- [13] Durrer R., Ferreira P. G. & Kahniashvili T. 2000, *Phys. Rev. D.*, 61, 043001
- [14] J.W. Dreher J. W., Carilli C. L. & Perley R. A. 1987, *Astrophys. J.*, 316, 611
- [15] Paoletti D., Finelli F. & Paci F. 2009, *MNRAS*, 396, 523
- [16] Finelli F., Paci F. & Paoletti D. 2008, *Phys. Rev. D*, 78, 023510
- [17] Jedamzik K., Katalinik V. & Olinto A. 1998, *Phys. Rev. D*, 57, 3264
- [18] Trivedi P., Subramanian K. & Seshadri T. R. 2013, *Phys. Rev. D*, 89, 043523
- [19] Kim E. J., Olinto A. & Rosner R. 1996, *Astrophys.J.*, 468, 28
- [20] Kahniashvili T. & Ratra B. 2007, *Phys. Rev. D.*, 75, 023002
- [21] Hortua H. J., Castañeda L. & Tejeiro J. M. 2013, *Phys. Rev. D.*, 87, 103531
- [22] Subramanian K. & Barrow J. D. 1997, *Phys. Rev. D.*, 58, 083502
- [23] Caprini C., Finelli F., Paoletti D., & Riotto A 2009, *JCAP*, 0906, 021
- [24] Hu W. & White M. 1997, *Phys. Rev. D.*, 56, 596